Possible remnants of a frozen mud lake in southern Elysium, Mars

Possible remnants of a frozen mud lake in southern Elysium, Mars.

Konrad J. Kossacki [a,b,*] Wojciech J. Markiewicz [c]
Michael D. Smith [d] David Page [e] John Murray [f]

[a] *Institute of Geophysics of Warsaw University, Pasteura 7,02-093 Warsaw, Poland*

[b] *Visiting scientist, Max-Planck-Institute for Solar System Investigations, Max-Planck-Str 2, D-37191 Katlenburg-Lindau*

[c] *Max-Planck-Institute for Solar System Investigations, Max-Planck-Str 2, D-37191 Katlenburg-Lindau, Germany*

[d] *NASA Goddard Space Flight Center, Greenbelt, MD 20071, USA*

[e] *Dept. of Mineralogy, The Natural History Museum, London SW7 5PB, U.K.*

[f] *Dept. of Earth Sciences, The Open University, Milton Keynes MK7 6AA, U.K.*

Abstract

In this work we estimate the maximum persistence time of subsurface ice in water rich sediment layers remaining after drying of a Martian lake. We simulate sublimation of ice from layers of different granulations and thicknesses. Presented results assume insolation and atmospheric conditions characteristic for the present day southern Elysium, where data from Mars Express have identified surface features possibly indicating the very recent presence of a frozen body of water (Murray *et al.*, 2005). The age of these features is estimated to be several million years. On this time scale, we find that most of the water ice must have sublimated away, however remnant ice at a few percent level can not be excluded. This amount of water ice is sufficient for chemical cementation of the observed features and explains their relatively pristine appearance, without significant signs of erosion.

Key words: Mars, Water

* Corresponding author
Email address: kjkossac@fuw.edu.pl (Konrad J. Kossacki).

1 Introduction

One of the images taken of southern Elysium by the High Resolution Stereo Camera onboard Mars Express shows intriguing features resembling those observed on ice covered Earth seas (Murray *et al.*, 2005). The authors have identified several kilometer-scale plates which resemble pack ice floating at the surface of a frozen ocean, see Fig.1. The available data however, do not say anything about the current composition of these structures. Of particular interest is whether water ice is still present there. Here we investigate the long term stability of water ice in this region assuming present day Martian climatic conditions. For comparison we also include a simulation with a much denser atmosphere, as may be appropriate for periods when Mars had a higher obliquity.

The analysed features are observed close to the equator, at 5^oN/150^oE. At this latitude, under present Martian climate conditions, surface temperatures prohibit the persistence of uncovered ice. However, buried subsurface ice sublimes more slowly, and should remain noticeably longer. Fine-grained sediments may effectively reduce sublimation due to low thermal conductivity and a low diffusion coefficient.

In this work we test the hypothesis of the frozen mud lake remaining after drying of a larger water basin. Fine-grained bottom sediments having a large water content would form an ice/dust mixture, on freezing. Subsequent sublimation would result in burial of ice under an insulating layer of growing thickness. It is however, unlikely that the ice table simply moves downward. Diffusing vapour may periodically recondense in the overlying dust layer, smoothing the profile of ice concentration versus depth. Re-freezing of ice higher up the sediment column affects local properties of the medium, its permeability and thermal conductivity. The former reduces the diffusion of the buried ice, but later may result in a significant increase of the heat flux conducted downward from the warmed surface. In the next section we describe the model used to consider the above problem. This is followed by presentation of results and discussion.

2 LWMRM

The Lindau-Warsaw-Mars-Regolith-Model (LWMRM) used in this work was initially applied to investigate the sublimation of water ice from the regolith at the planned landing side of the Mars Polar Lander (Kossacki *et al.*, 2001). In subsequent applications of LWMRM we improved its accuracy, allowed for more complex geometries and implemented more physical processes (Kossacki and Markiewicz, 2002; Kossacki *et al.*, 2003). The latest version (Kossacki

and Markiewicz, 2004) was used to investigate the possibility of seasonal ice melting in the Martian gullies. LWMRM calculates the seasonal cycle of the heat and vapour transport within the porous regolith, including sublimation and recondensation of both water and carbon dioxide. In the past applications of LWMRM the surface water vapour was prescribed from the results of the General Circulation Model. This was a sensible although not self-consistent approach, since we were interested in modelling the present Mars climate and its seasonal cycle. Here we are interested in much longer time-scales, where the atmospheric water vapour content is not known. We decided to keep this parameter constant at 10 precipitable microns in simulations dealing with current climate conditions, and at 100 precipitable microns in simulations dealing with periods of higher obliquity, where we also assume the atmosphere to be five times denser than at present.

Thermal conductivity of the medium is calculated assuming a granular structure, accounting for the contact areas of the grains, which in turn is related to the porosity. The conductivity of the dry (dust) matrix is estimated from a fit to the Thermal Emission Spectrometer (TES) Christensen *et al.* (2001) surface temperature data (see below). Condensation and sublimation of the ice within this matrix modifies this conductivity according to how much ice is present at any particular time and place. The model includes single scattering of solar radiation in the atmosphere. This was enough to reproduce measured surface temperatures at high latitudes (Kossacki *et al.*, 2003). In the current version of the model we have also added simple parameterisation of the IR emission in the atmosphere, to account for the changes of atmospheric opacity by a factor of two, or more, on the seasonal scale, as indicated by the TES observations for quiet years (Smith, 2004). The flux of IR radiation emitted toward the surface is

$$F_{atm} = s_0 + s_1 F_{solar,max} (\tau/\tau_0)^2, \tag{1}$$

where $F_{solar,max}$ is the diurnal maximum of the direct solar radiation reaching the surface. This formula is based on that used by Palluconi and Kieffer (1981). The coefficients s_0, s_1 and τ_0 are fitted together with the thermal inertia I of the ice free soil, using the seasonal profiles of day and night TES surface temperatures.

The ice/dust layer in the calculations discussed below has thickness L within the range 5 - 20m. This is at least a factor of two thinner than the depth estimated in Murray *et al.* (2005). Unfortunately, for computational reasons we are limited to 20 meters, but we have developed methods to extrapolate the calculated results to deeper layers. This is discussed towards the end of the results section. The radii of the mineral grains r_g are within the range 1 - 5 μm. The near surface atmospheric pressure is taken from the Global atmospheric Circulation Model (GCM) (Forget *et al.*, 1999; Lewis *et al.*, 1999).

The atmosphere is assumed to be moderately dusty, with the visual opacity given by the TES data collected during periods without global dust storms (Fig. 2). The algorithm used during processing of TES measurements is described in Smith (2004) and references therein. With the profile of atmospheric opacity, as shown in Figure 2, we calculated diurnal and seasonal evolution of the surface temperature. The results are fitted to the TES surface temperatures measured in the region 4 - 6^oN and 149 - 151^oE. The free parameters of this fit are thermal inertia of the surface material, surface albedo and the three coefficients in eq. 1. We obtain satisfactory agreement when the thermal inertia I is within the range $100 - 200 \mathrm{J\,m^{-2}\,K^{-0.5}\,s^{-0.5}}$ and the remaining parameters have the following values:, $s_0 = 15 \mathrm{W\,m^{-2}}$, $s_1 = 0.025$, $\tau_0 = 0.5$ and $A = 0.23$. The model fits are compared to TES temperatures in Fig. 2. The night temperature is well reproduced by the model, while the simulated day time temperature is, in the dusty season ($\mathrm{L}_s > 240$), noticeably lower than that retrieved from TES observations. This periodical bias could be due to warming of the surface by wind, and is not included in our model. The resulting small disagreement of seasonally averaged temperature may cause a slight overestimate of ice persistence time. On the other hand, exact agreement with TES data is not critical for long-term simulations, because we do not know the past values of various parameters, including atmospheric opacity. The estimated flux F_{atm} is in satisfactory agreement with the values predicted by the GCM model. Our estimate of thermal inertia of the regolith matches that found previously from TES data. According to Mellon *et al.* (2000), the region around 5°N and 150°E should be characterized by thermal inertia somewhat below $200 \mathrm{J\,m^{-2}\,K^{-0.5}\,s^{-0.5}}$. In the past, thermal inertia was probably much higher. As long as ice is in the soil it has a significant influence, masking the properties of the non-volatile mineral component. Thus, for our study of ice-containing regolith, the properties without ice have only moderate importance. Nevertheless, we have performed simulations assuming different values of I. If it is not stated otherwise, we use the value $230 \mathrm{J\,m^{-2}\,K^{-0.5}\,s^{-0.5}}$, corresponding to the thermal conductivity of an ice-free sediment layer $\lambda_r = 50$ $\mathrm{mW\,m^{-1}\,K^{-1}}$, when the bulk thermal conductivity is 4.2 $\mathrm{W\,m^{-1}\,K^{-1}}$. These values indicate the dimensionless volume of mineral component $v_r/v = 0.54$, hence the porosity $\psi = 0.46$.

3 Results

The simulations discussed here are very computationally intensive. The computation time is strongly dependent on the size of the numerical grid and its resolution. We have minimized the resolution (grid spacing is 50 cm) to be able to model deeper layers. Tests with higher resolution grids show that the results here are correct, at least within a factor of two. Even with this low

resolution we are still limited to layers not deeper than 20 meters. Below, we show how results obtained for 5, 10 and 20 meters can be extrapolated, with some caution, to larger values.

We assumed that the initial volume of ice increases linearly from zero at the surface to the maximum at the initial position of the ice table, which is 2 meters below the surface. The frozen layer has finite thickness as given above and has an impermeable bottom. We expect that the process of ice sublimation will have two phases. During the first, the ice table moves downward; later, ice sublimes form the whole layer. The sublimation of ice does not affect the volume of the medium. The remaining non-volatile component of the sediment has the dimensionless volume v_r/v, corresponding to the cubic structure of spherical grains flattened at the contacts. The areas of grain-to-grain contact surfaces are adjusted so that the thermal conductivity has the value as obtained in the previous section.

Fig. 3 shows evolution of the dimensionless volume of water ice v_{ice}/v versus time at different depths in the 5 meter deep layer, for two values of the grain radius $r_g = 5\mu$m, and 1μm. It can be seen that the ice volume fraction reaches levels of less than one percent in about a thousand Martian years. The dependence on the grain radius is not very strong. The pores have radii equal to, or smaller than, r_g, depending on the local content of ice.

The first phase of sublimation is relatively short. The ice table reaches the bottom of the mud layer after about 100 Martian years. This can be best seen in Figure 4 where the ice volume fraction is plotted this time against depth for several different time values. Note that results shown in this figure are for the 10 m layer. After the ice table reaches the bottom of this layer, ice continues to sublime from the whole layer. As the volume of ice decreases, porosity and pore radii increase, enhancing the vapour diffusion coefficient. The whole layer becomes free of ice to a level of a few percent after about 4×10^3 Martian years. The rate of sublimation depends mostly on the energy transport into the regolith, and hence, on the current effective thermal conductivity. Figure 5 shows profiles of the effective thermal conductivity $\lambda_{\rm eff}$ versus depth also for the 10 meter deep layer. The curves are drawn for the same time values as those for the volume ice fraction in Fig.4. It can be seen that, $\lambda_{\rm eff}$ is a strong function of ice content. As the layer loses its ice, the thermal contact between the dust particles weakens, porosity increases, and $\lambda_{\rm eff}$ decreases. This in turn means that the rate of sublimation and loss of the ice from the layer always decreases. This can be seen in Figures 3 and 6, although it is somewhat masked by the log-log plot. Figure 6 shows the evolution of the ice volume fraction at various depths for both the 10 m and 20 m deep layers. The ice volume fraction reaches the few percent level for the 20 m layer after several tens of thousands of Martian years.

As mentioned above, for computational reasons, we are able to model layers up to 20 m deep. We can however, find an analytical estimate of the ice sublimation rate. For the vapour flux from the bottom of the layer we can write

$$F_{\mathrm{v}} = F_{\mathrm{heat}} H^{-1} = \lambda \frac{\Delta T}{L} H^{-1}, \tag{2}$$

where F_{v} is the vapour flux, F_{heat} is the heat flux and H is the latent heat of sublimation. Using Eq.2 it is possible to define the time scale of sublimation as a function of thermal properties of the regolith

$$t_{\mathrm{subl}} = \left(\frac{dz_{\mathrm{i}}}{dt}\right)^{-1} L = \left(\lambda_{\mathrm{eff}} \frac{\Delta T}{L} H^{-1} \varrho_{\mathrm{i}}{}^{-1}\right)^{-1} L = \frac{L^2 \varrho_{\mathrm{i}} H}{\lambda \Delta T}, \tag{3}$$

where ϱ_{i} is the bulk density of ice. The key parameter λ_{eff} depends mostly on the ice content in the pores, as already discussed above in the context of Figures 4 and 5. Only when ice is present at a depth lower than L, can we assume that $\lambda_{\mathrm{eff}} = \lambda$, the thermal conductivity of the dry regolith. If we take $L = 5$ m, the surface temperature $T_s = 280$K, the temperature at the depth of 5m $T_{bottom} = 200$K, and the thermal conductivity $\lambda = 50\mathrm{mW\,m^{-1}\,K^{-1}}$ we get $t_{subl} = 400$ Martian years. This is in good agreement with the simulations of the 5 m layer (Figure 3). For the layer of $L = 20$m, according to Eq.3 we should expect $t_{subl} = 6.4\,10^3$ Martian years, when $\lambda = 50\mathrm{mW\,m^{-1}\,K^{-1}}$, or t_{subl} $= 6.4\,10^5$ Martian years when $\lambda = 5\mathrm{mW\,m^{-1}\,K^{-1}}$.

The above estimate ignores the depth dependence of the thermal conductivity. Indeed, in the porous material containing ice λ_{eff} strongly depends on the temperature and the local ice content. This is due to the temperature dependence of the thermal conductivity of ice itself, but also due to the heat transport related to the local sublimation and recondensation. The formula for the effective thermal conductivity can be written as,

$$\lambda_{\mathrm{eff}} = \lambda + \lambda_{\mathrm{i}} h(v_{\mathrm{i}}) \frac{v_{\mathrm{i}}}{v} + r_p(v_{\mathrm{i}}) \psi(v_{\mathrm{i}}) \left(\frac{8\mu}{9\pi RT}\right)^{0.5} H \left|\frac{dp_{\mathrm{sat}}/dT}{dT/dz}\right|, \tag{4}$$

where h is the Hertz factor describing the grain to grain contact area, λ_{i} is the bulk thermal conductivity of ice, ψ is the porosity and p_{sat} is the vapour saturation pressure. Except for a thin near surface layer, the temperature does not exceed 200K. This makes the last term in Eq. 4 negligible. However, the function $h(v_{\mathrm{i}})$ can have values from as low as almost zero to near unity. When the ice free deposit has $\lambda = 50\mathrm{mW\,m^{-1}\,K^{-1}}$ and thus $h(v_{\mathrm{i}}/v = 0) = 0.022$, our model predicts $h(v_{\mathrm{i}}/v = 0.02) = 0.05$, $h(v_{\mathrm{i}}/v = 0.15) = 0.2$ and $h(v_{\mathrm{i}}/v = 0.4) = 0.64$. When $v_{\mathrm{i}}/v = 0.02$ and $T = 200$K, Eq.4 gives $\lambda_{\mathrm{eff}} = 55\mathrm{mW\,m^{-1}\,K^{-1}}$, only 10%

larger than λ and at $T = 220\mathrm{K}$ $\lambda_{eff} = 90\mathrm{mW\,m^{-1}\,K^{-1}}$. Thus, when the amount of ice is small, thermal conductivity λ_{eff} is not significantly higher than λ, except at very small depths.

Given this rough agreement of Eq. 3 with the calculations for layers of depth up to 20 m we will now attempt to extrapolate these results for deeper layers. Figure 7 shows the square root of the time it takes to reach a certain level of ice in the layer as a function of depth of the layer. It can be seen that the estimate according to Eq. 3 agrees well with the calculated values when the final ice volume fraction is in the range of 2%-5%. The calculated values diverge in opposite directions away from the quadratic dependence of t_{subl} on L outside of this range. The extrapolation for a 50 m deep layer indicates that it will take about 3×10^4 Martian years for the ice to be reduced to a few percent per volume. It also shows however, that traces of water will persist within the layer for a time scale of the order of 10^5 Martian years. This timescale is an order of magnitude smaller than the estimate of the age of the pack ice observed in the HRSC images.

Finally, the estimate of the persistence time of ice, as discussed above, should be considered only as a rough estimate, nevertheless useful. The presence of even a very small amount of water ice over the age of these features would ensure a stronger cohesive strength of the material and explain the relatively sharp boundaries observed. The sublimation of ice from the considered deposit does not lead to the formation of an ice-free layer of growing thickness. Instead, during most of this time, the concentration of ice decreases at all depths. This process transforms the frozen muddy matter into a porous regolith of mineral grains bounded by remnant ice. As the amount of ice decreases, the mechanical strength of the medium may be sufficient to prohibit gravitational collapse, or slow self-compression. If any compression does take place, the volume concentration of ice will increase, reducing porosity, and hence slowing further escape of ice to the atmosphere.

4 Discussion

One of the key assumptions of the model used to obtain the results described above is that of current martian climatic conditions throughout the period of calculation. It is however, much more likely that on the long time scales considered, the Martian climate has been very different. It is well known that the obliquity of Mars changes in a chaotic fashion with various periodicities (Laskar and Robutel , 1993; Touma and Wisdom, 1993). Within the last five million years, Martian obliquity has oscillated between about 15 and 35 degrees. Earlier than five million years ago, it oscillated with similar amplitude, around a value of nearly 40 degrees. Since the region of Mars studied in this

work could have components (plates) as young as five million years (Murray *et al.*, 2005), it is of interest to consider the impact of obliquity change on the results presented above. It is also possible, if not likely, that during the higher obliquity period, Mars had a much thicker atmosphere. To assess the significance of these potential differences, we have calculated a model with an obliquity of 40° and a rather dense atmosphere with surface pressure equal to 500 Pascals. The results of this simulation are shown in Figure 8. The calculation was performed for a 5 m thick layer and the curves in Figure 8 should be compared with those in the top panel of Figure 3. We can see that ice is stable for a period about 50 times longer in the case of the thicker atmosphere and large obliquity. Extrapolating this result for the 50 m thick layer would result in stability of ice at at least the few percent level for periods in excess of a million Martian years. This last value is comparable to the age of this presumed remnant frozen lake.

There are at least two more processes not considered in the present work that could further increase the timescale of the stability of water ice within the deposit. Firstly, the layer at the time of freezing could have been thicker than at present. Sublimation of ice in the upper layers could lead to its collapse. This in turn would increase the volume fraction of ice. It is also possible that the frozen layer was covered by an additional layer of the fine-grained dust or volcanic ash. Such layer may have very low thermal conductivity and permeability. If it was deposited under climatic conditions prohibiting condensation of atmospheric water this fine grain layer should remain ice-free. Skorov *et al.* (2001) have shown that a layer of this type is a very effective insulator for water ice. Unfortunately, their calculations are for high latitudes only and it is not clear to what degree they can be applied to the equatorial regions.

All of the results presented here are consistent with the region discussed by Murray *et al.* (2005) as a remnant frozen lake. The exact amount of ice still present today is probably not much more than a few percent by volume. It is significant however, that the water ice is distributed throughout the layer at all times during the sublimation period. It is not just a simple ice table, the level of which moves downward with time. This is important for the material strength of the layer, its chemistry, and hence long term preservation of the observed topography with well defined boundaries.

5 Acknowledgments

This research was in part supported by the grant MA1871/1-2 of the German Research Foundation (DFG), and in part by the grant No 2P03D 01025 provided by polish Ministry of Scientific Research and Information Technology.

References

Christensen P. R. and 25 co-authors 2001. Mars Global Surveyor Thermal Emission Spectrometer experiment: Investigation description and surface science results. *J. Geophys. Res.*, 106, E10, 23823–23871

Forget, F., F. Hourdin, R. Fournier, C. Hourdin, O. Talagrand, M. Collins, S. R. Lewis, P. L. Read, and J. Huot 1999. Improved general circulation models of the Martian atmosphere from the surface to above 80 km. *J. Geophys. Res*, 104, 24,155–24,176.

Kossacki, K.J., W.J. Markiewicz, and H. U. Keller 2001. Efect of Surface Roughness on Ice Distribution in the South Subpolar Region of Mars. *Planetary and Space Science*, 49, 437–445

Kossacki, K.J.and W.J. Markiewicz 2002. Martian Seasonal CO_2 Ice in Polygonal Troughs in Southern Polar Region: Role of the Distribution of Subsurface H_2O Ice *Icarus*, 160, 73–85

Kossacki, K.J., W.J. Markiewicz, and M. D. Smith 2003. Surface temperature of Martian regolith with polygonal features: influence of the subsurface water ice. *Planet. Space Sci.*, 51, 569–580

Kossacki K. J., and W. J. Markiewicz 2004. Seasonal melting of surface water ice condensing in Martian gullies. *Icarus*, 71, 272–283

Lewis, S. R., M. Collins, P. L. Read, F. . Forget, F. . . Hourdin, R. Fournier, C. Hourdin, O. Talagrand, and J. Huot, A climate database for Mars 1999. *J. Geophys. Res*, 104, 24,177–24,194

Mellon, Michael T., B.M. Jakosky, H.H. Kieffer and P.R.Christensen 2000.. High-Resolution Thermal Inertia Mapping from the Mars Global Surveyor Thermal Emission Spectrometer. *Icarus*, 148, pp. 437–455

Murray J.B., J. Muller, G. Neukum, E. Hauber, W.J. Markiewicz, J. W. Head III, B. H. Foing, D. Page, K.L. Mitchell, G. Portyankina and the HRSC Co-Investigator Team 2005. Evidence from the Mars Express High Resolution Stereo Camera for a frozen sea close to the Mars equator. *Nature*, 434, pp. 352–356

Palluconi F. D. and H. H. Kieffer 1981. Thermal inertia mapping of Mars from 60 deg S to 60 deg N. *Icarus*, 45, pp. 415–426

Skorov Y. V., W.J. Markiewicz, A.T. Basilevsky, and H.U.Keller 2001. Stability of water ice under a porous nonvolatile layer: implications to the south polar layered deposits of Mars. *Planetary and Space Science*, 49, pp. 59–63

Smith M. D. 2004. Interannual variability in TES atmospheric observations of Mars during 1999-2003. *Icarus*, 167, 148–165

Touma J., Wisdom J. 1993. The chaotic obliquity of Mars. *Science*, **259**, 1294–1297

Laskar J., Robutel P. 1993. The chaotic obliquity of the planets. *Nature*, **361**, 608–612

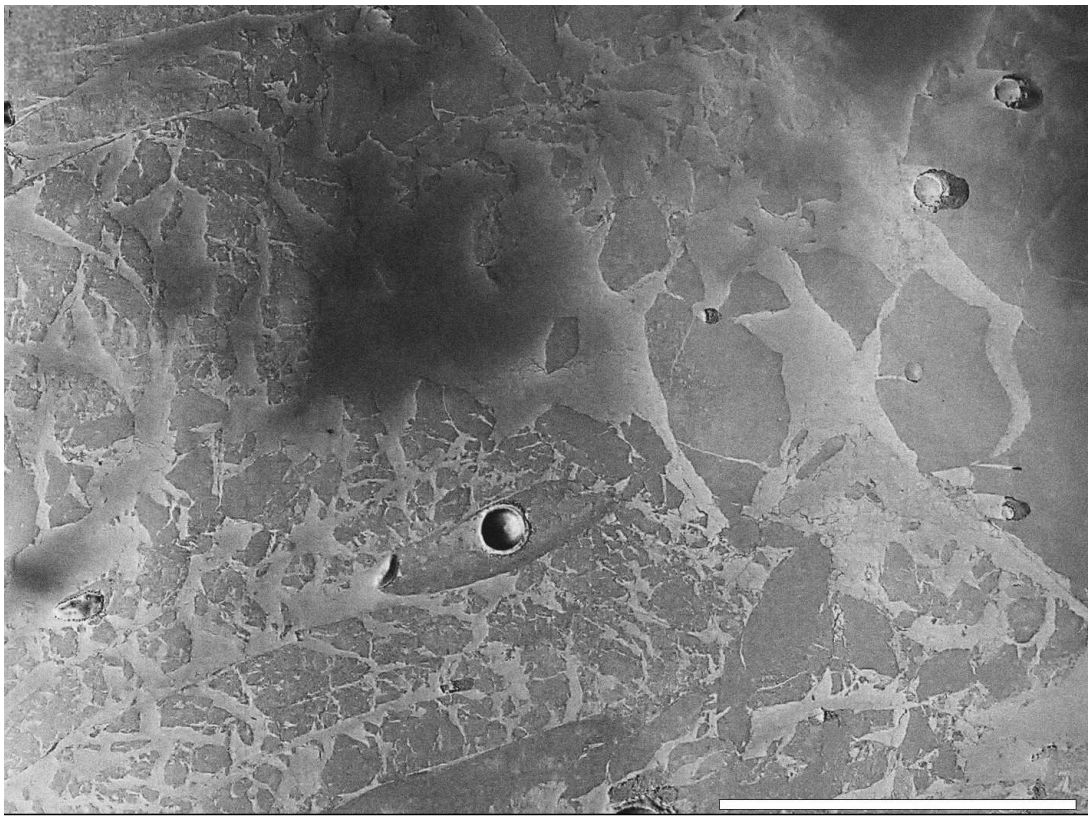

Fig. 1. Part of Mars Express High Resolution Stereo Camera image showing fractured plates resembling pack-ice in Elysium Planitia, from Murray *et al.* (2005). The centre of the image is near longitude 150 degrees east, latitude 6 degrees north, and the scale bar (lower right) is 25 km.

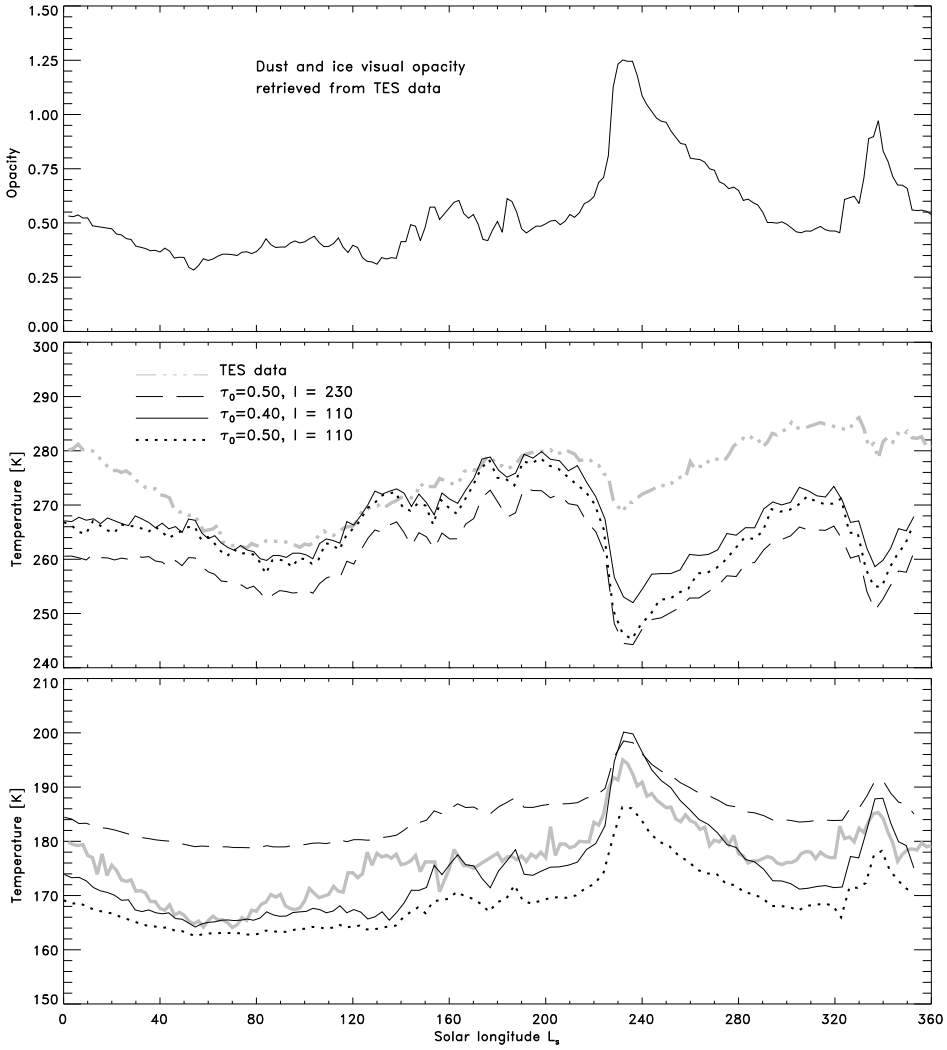

Fig. 2. Atmospheric opacity for a quiet year as retrieved from TES data (top). Corresponding surface temperature, TES data (gray lines)and simulated assuming different parameters (black lines). Plotted are temperature profiles at 14:00 (middle panel) and 2:00 (bottom panel).

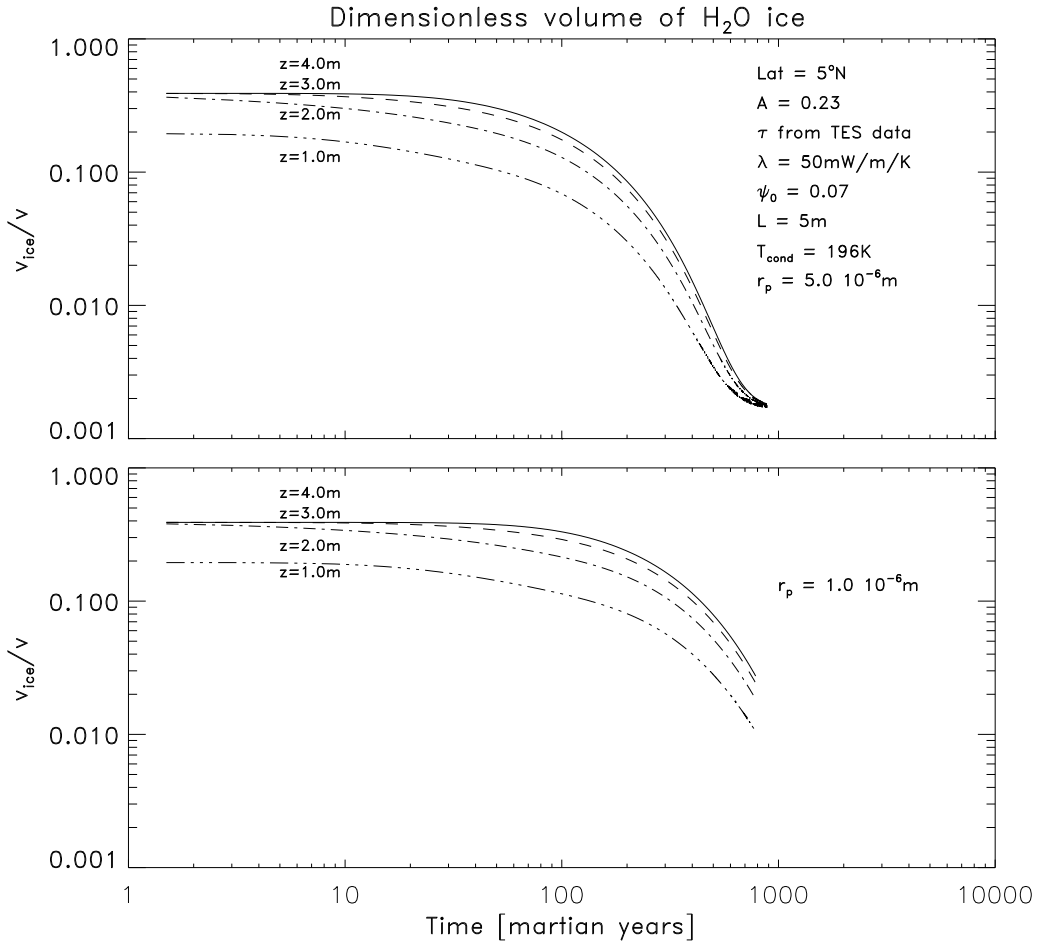

Fig. 3. Volume fraction of water ice as a function of time and for several depths. Layer is 5 m thick. The radius of grains in the regolith is 5 micron (top) and 1 micron (bottom).

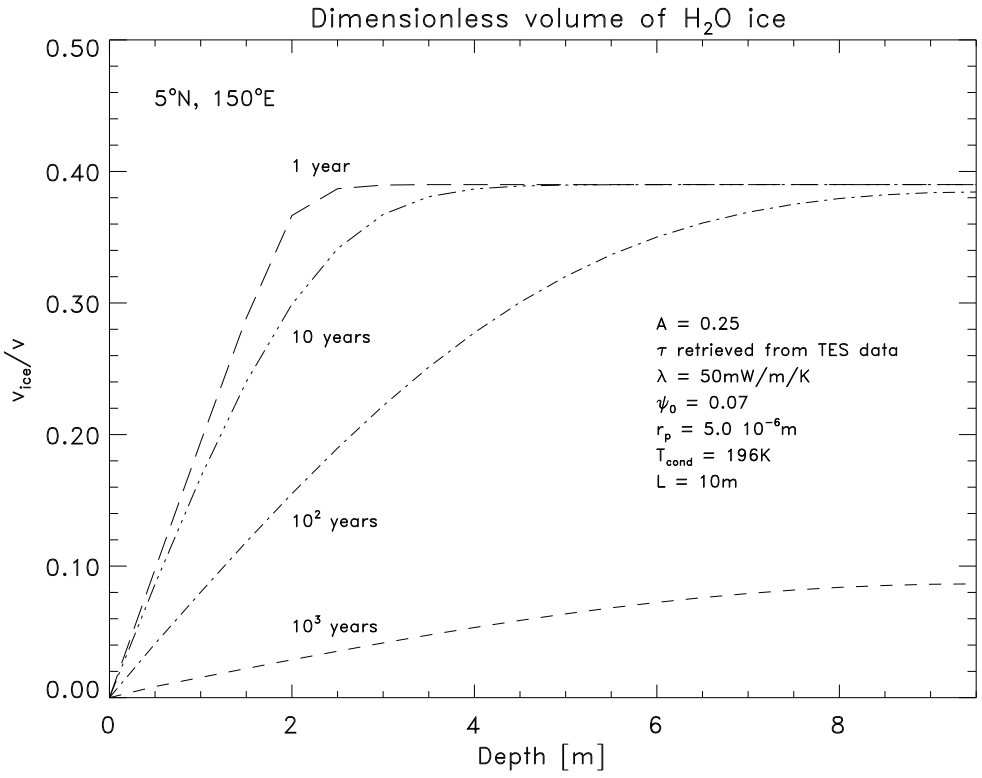

Fig. 4. The volume fraction as a function of depth within the 10 m thick layer.

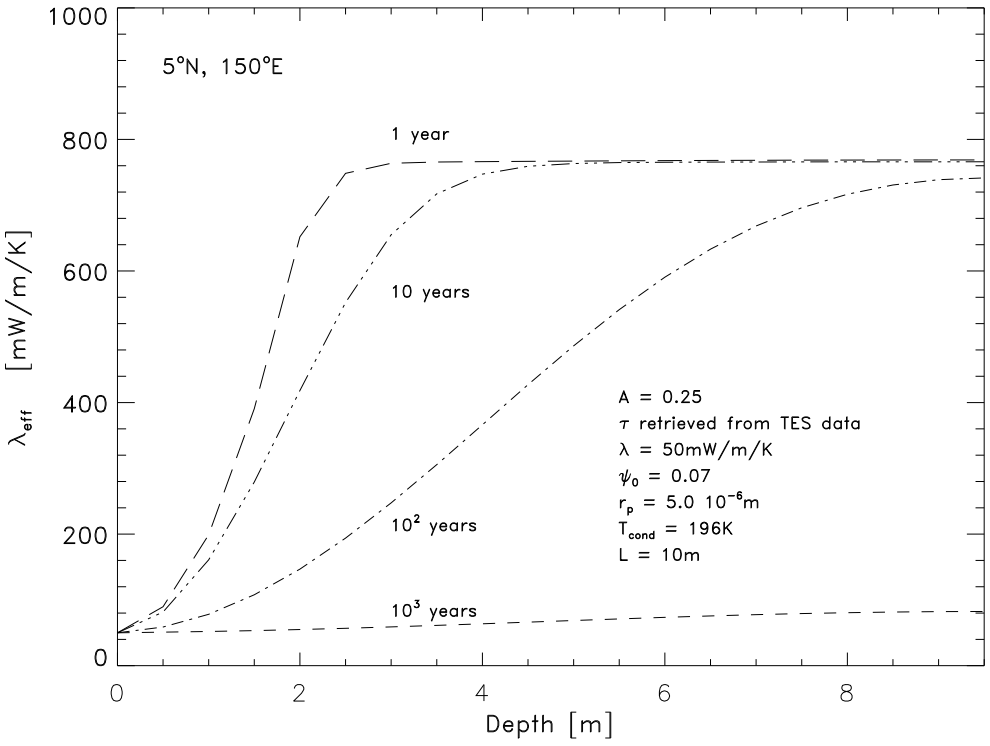

Fig. 5. As Figure 4 but for effective thermal coductivity.

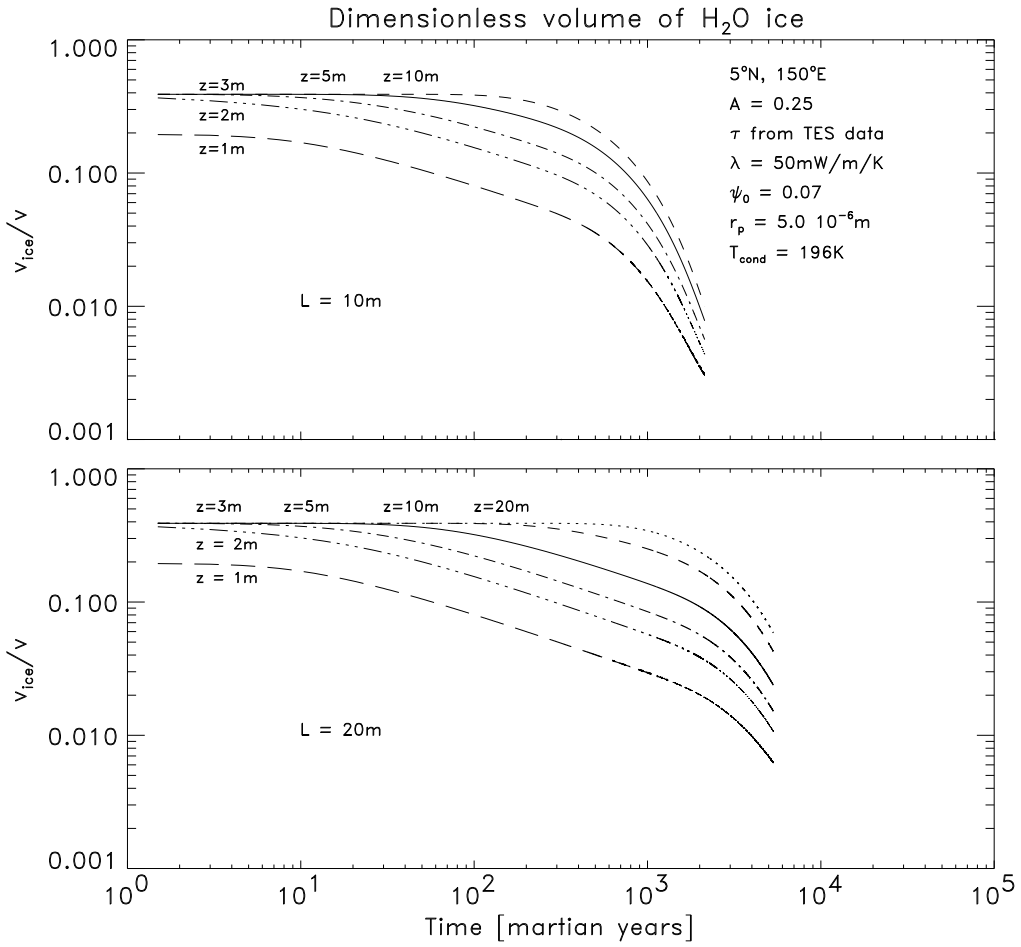

Fig. 6. As top panel of Figure 3, but for layer 10 m thick (top) and 20 m thick (bottom)

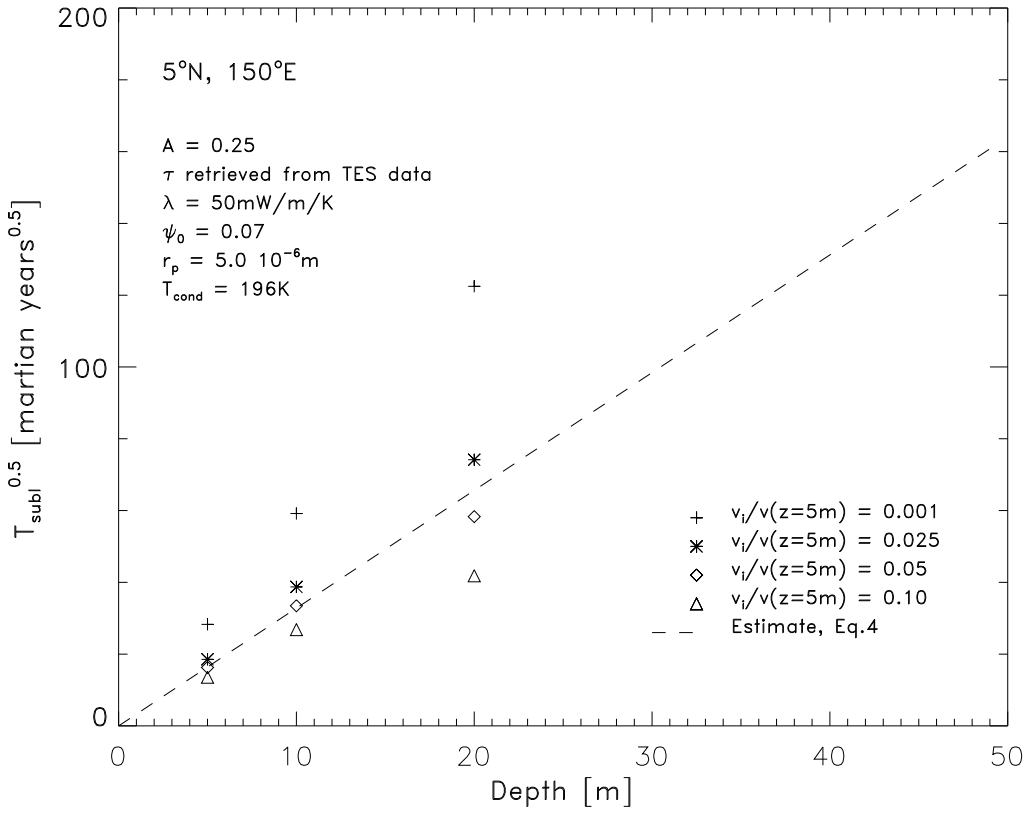

Fig. 7. Time to decrease water ice volume fraction to a particular value, for various depths. Dashed line corresponds to Eq. 3

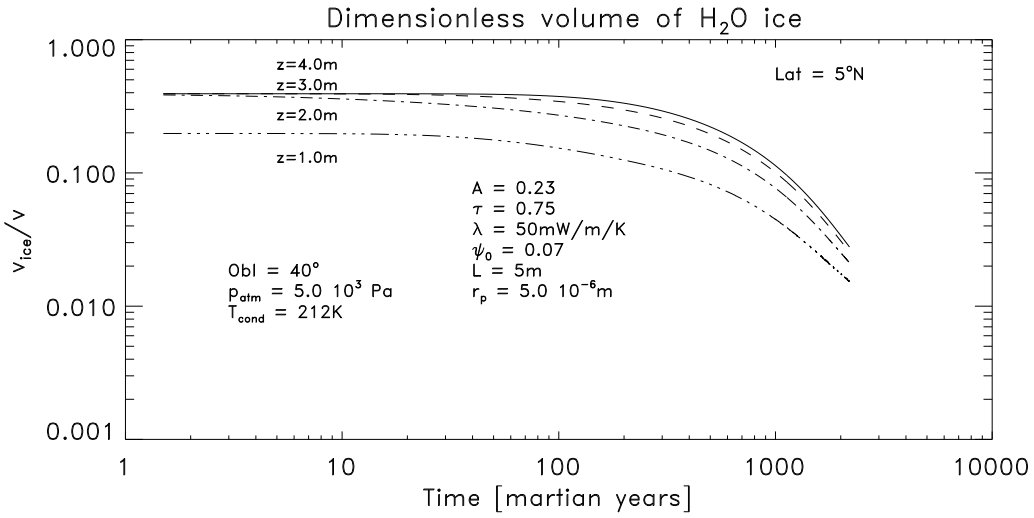

Fig. 8. As top panel of Figure 3 but for thick atmosphere and high obliquity.